Soils and Rocks
www.soilsandrocks.com
An International Journal of Geotechnical and Geoenvironmental Engineering
ISSN 1980-9743
ISSN-e 2675-5475

# Shear strength of an unsaturated laterite soil under different compaction conditions

Ivan Fernando Otálvaro[1], Vinícius de Oliveira Kühn[2#], Bruno Leite Ramires Saldanha[3], Bernardo Caicedo[4], Manoel Porfírio Cordão Neto[3]

Article

**Keywords**
Compacted soil
Tropical soil
Soil structure
Shear strength
Unsaturated soil

**Abstract**

Compacted soils are a common component of engineering structures worldwide. In tropical regions, lateritic soils exhibit distinct characteristics due to soil aggregation from iron and aluminum hydroxides and their bimodal structure. However, the compaction process can alter soil structure and mechanical behavior. This paper aims to assess the effects of soil structure on the saturated and unsaturated mechanical behavior of a lateritic soil under different compacted energies. The methodology involves porosimetry, retention curve and saturated and unsaturated triaxial tests, using appropriate standards and references. Under saturated conditions, these structural variations affected the volumetric behavior at the critical state, particularly in samples compacted on the dry side of the compaction curve. Additionally, a unique Critical State Line (CSL) could be traced for all samples in the $p'$ x $q$ space. Under unsaturated conditions, the effects of soil structure were evident, with both the volumetric response and shear strength increase being influenced by suction. Samples molded with no compaction energy, or non-proctor energy, resulted in higher macropore void ratio leading to more pronounced volumetric contraction during shear and less gain in shear strength. Therefore, this work contributes to the understanding of the behavior of compacted laterite soils, providing valuable information for projects involving compacted laterite soils in the field, such as dams, embankments and pavement subgrade.

## 1. Introduction

Soil compaction is a common practice in most of the geotechnical structures and is fundamental to understanding the hydromechanical behavior of soils (Kodikara et al., 2018). The behavior of compacted soils is typically represented by the compaction curve, which correlates the soil's water content with its dry density. Compaction is a crucial process in geotechnical engineering as it identifies the water content, optimum water content, which corresponds the maximum dry density of the soil for the tested soil at a specific compaction energy, thereby enhancing certain soil properties.

In the field, soils are usually compacted at their optimum water content. However, different water contents can also be used to achieve specific conditions, such as decreased compressibility, increased shear strength and reduced permeability. These effects are due to variations in void ratio and changes in soil structure resulting from the compaction process (Lambe, 1958; Lambe & Whitman, 1969).

The behavior of soil is also influenced whether it is compacted on the dry side or the wet of the compaction curve. Soils compacted on the dry side, or at the optimum water content, usually exhibit a bimodal pore size distribution (with two dominant pore sizes), while soils compacted on the wet side display a unimodal distribution, with only one dominant pore size (Delage et al., 1996; Tarantino & De Col, 2008). In contrast, previous research has shown that lateritic soils display a bimodal pore distribution regardless of the soil preparation method (Kühn et al., 2021; Ng et al., 2020) or compaction condition (Otálvaro et al., 2016; Santos & Esquivel, 2018).

Lateritic soils are widely distributed across many tropical regions and possess distinct structural characteristics due to weathering (Camapum de Carvalho & Gitirana, 2021). These soils are characterized by the agglomeration of the grains resulted

#Corresponding author. E-mail address: vinicius.kuhn@ufob.edu.br
[1]Pontificia Universidad Javeriana in Cali, Cali, Colombia.
[2]Universidade Federal do Oeste da Bahia, Centro das Ciências Exatas e das Tecnologias, Barreiras, BA, Brasil.
[3]Universidade de Brasilia, Departamento de Engenharia Civil e Ambiental, Faculdade de Tecnologia, Brasília, DF, Brasil.
[4]Universidad de Los Andes, Departamento de Ingeniería Civil y Ambiental, Bogotá, Colombia.

Submitted on April 28, 2025; Final Acceptance on November 27, 2025; Discussion open until November 30, 2026.
Editor: Renato P. Cunha
https://doi.org/10.28927/SR.2026.007025

from their mineralogy, primarily composed of aluminum and iron oxide, which defines their structure (Kühn et al., 2021; Miguel & Bonder, 2012; Mitchell & Soga, 2005; Otálvaro et al., 2016).

Over the years, several studies have been published to enhance the understanding of the relationship between soil structure and its mechanical behavior (Alonso et al., 2013, 1999; Burland, 1990; Cordão Neto et al., 2018; Delage et al., 2006; Dong et al., 2025; Kühn et al., 2022; Leroueil & Vaughan, 1990; Li et al., 2020; Nie et al., 2023; Ng et al., 2017; Prashant & Penumadu, 2007; Xu et al., 2025; Yu et al., 2016). The residual shear strength of saturated soils does not appear to be affected by the initial soil structure. (Tarantino & Tombolato, 2005; Wheeler & Sivakumar, 2000). The Soil Water Retention Curve (SWRC) also changes under different compactions condition (Fredlund et al., 2012), showing increased shear strength with increased suction (Vanapalli et al., 1996). Gui & Yu (2008) demonstrated that the sample preparation method, whether reconstituted or intact, of lateritic soil also influences the increase in shear strength with suction ($\phi^b$), with intact samples exhibiting higher shear strength. Futai & Almeida (2005) observed an increase in the Critical State Line (CSL) slope of intact tropical soil samples as suction increased.

Although several studies on lateritic soils have been published in recent years, there are still very few that examine the effects of compaction on the structure of lateritic soils and their mechanical behavior. Therefore, the objective of this study is to assess the impact of soil structure on the saturated and unsaturated shear strength of lateritic soils under different compaction conditions. The soil structure will be characterized using Mercury Intrusion Porosimetry (MIP) test and Soil Water Retention Curve (SWRC) tests on samples compacted on both proctor and non-proctor energies. Shear strength will be evaluated through saturated and unsaturated triaxial tests on samples with varying structures, enabling a correlation between pore distribution, water content, and mechanical behavior.

## 2. Methods and materials

### 2.1 Samples preparation

The soil used in this research was a tropical soil from Distrito Federal, Brazil, classifies as low plasticity silt (ML) according to the Unified Soil Classification System (USCS) (Otálvaro et al., 2016, 2015). The liquid limit ( $w_l$ ) is equal to 40%, the plasticity Index (*PI*) is 12% and the soil specific gravity ($G_s$) is 2.76. XRD tests on the soil revealed the presence of 42-50% of kaolinite, 18-20% de gibbsite, 16-22% de quartz, 4-9% illite, 4-8% goethite and 1-10% de hematite (Martins, 2000).

Figure 1 shows the particle size distribution obtained through sieving and laser diffraction, both with and without the use of dispersing agents (sodium hexametaphosphate). The laser method offers a broader range of detectable particle sizes and better accuracy in the micron and submicron ranges compared to the sieve method (Di Stefano et al., 2010). The particle size distribution obtained using the dispersant showed a higher content of silt and clay compared to the curve obtained without a dispersant. This result is expected due to the tendency of tropical soils to have a high degree of particle aggregation (Kühn et al., 2021; Ng et al., 2020; Otálvaro et al., 2015; Miguel & Vilar, 2009; Miguel & Bonder, 2012).

Sample preparation consisted of air-drying, crushing and homogenizing, followed by humidifying the samples for 24 hours and compaction using standard Proctor energy (ASTM, 2012). The compaction curve was used to define three samples compacted under different conditions to achieve various soil structures. Sample PN20 was compacted on the dry side ($w$=20%, $\gamma_d$=14kN/m$^2$), Sample PN24 was compacted at the optimum water content ($w$=24%, $\gamma_d$=15N/m$^2$), and Sample PN28 was compacted on the wet side ($w$=28%, $\gamma_d$=14kN/m$^2$). A fourth sample, NP24, was molded at the optimum water content, but was not compacted ($w$=24%, $\gamma_d$=13.9kN/m$^2$) allowing to evaluate any soil characteristics resulting from a non-proctor compaction procedure. The purpose of the non-proctor condition is to observe the behavior of the soil if it is not properly compacted in the field. Figure 2 shows the resulting compaction curve.

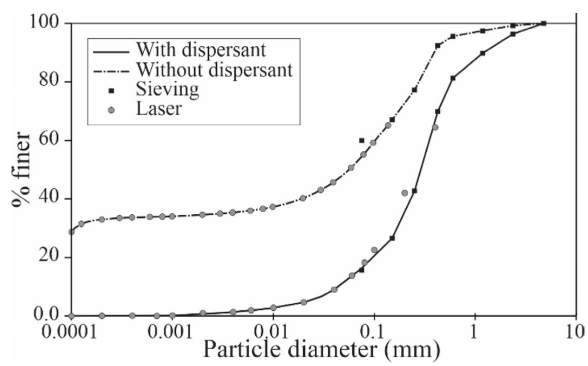


**Figure 1.** Particle size distribution of the samples with and without dispersing agents (Modified from Otálvaro et al., 2015).

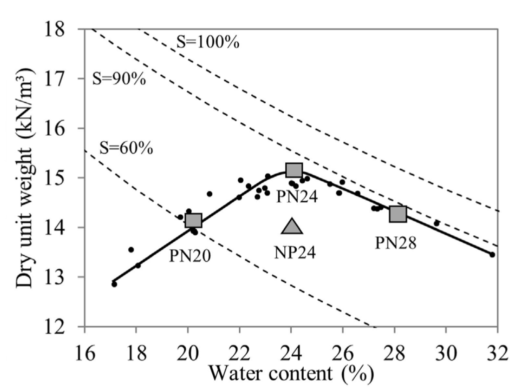


**Figure 2.** Compaction Curve obtained for the sample (Modified from Otálvaro et al., 2015).

### 2.2 SWRC and MIP tests

The soil water retention curves (SWRC) were obtained through various drying trajectories and tests. Suction values below 16 kPa were measured using suction plate tests, for values above 16 kPa were determined using the filter paper method.

The suction plate involves applying negative head, with air pressure maintained atmospheric conditions. The filter paper method followed the procedure outlined by Marinho & Oliveira (2006), using calibration equations for Whatman No. 42 paper as described by Chandler et al. (1992). The procedure for measuring matric suction by the method consists of intimate contact between the filter paper and the soil and an equilibration time of 14 days. The resulting curves were then fitted using the van Genuchten (1980) equation, considering two pore size distributions, as proposed by Durner (1994), Equation 1.

$$e_w = \frac{e_w^L}{\left[1+(a_L.S)^{n_L}\right]^{1-1/n_L}} + \frac{e_w^s}{\left[1+(a_S.S)^{n_s}\right]^{1-1/n_s}} \quad (1)$$

where: $a$ and $n$ are fitting parameters, $S$ is suction, L and s subscriptions stand for large and small respectively, $e_w$ is the water index, i.e., volume of water / volume of solids.

The Mercury Intrusion Porosimetry (MIP) teste was performed by an AutoPore IV 9500 on samples with a diameter of 8 mm and a height of 10 mm. The samples were frozen with liquid nitrogen and freeze-dried, as described by Otálvaro et al. (2016). Pore diameters were obtained from the mercury intrusion curve using the equation from Diamond (1970), with a contact angle of 140º between the material and mercury and a mercury surface tension of 0.484 N/m (Diamond, 1970). considering a contact angle between the material and mercury of 140º and a superficial stress of 0.484 N/m (Diamond, 1970). The mercury intrusion data were analyzed using the equations proposed by Durner (1994) and Lopes et al. (2014), equation 2, allowing for the determination of macropore ($e_{macro}$) and micropore ($e_{micro}$) pore void ratios. The $R^2$ correlation coefficient ranged from 0.98 to 1.00.

$$e_{MIP} = \frac{e_{macro}}{\left[1+(D/d_{macro})^{n_{macro}}\right]^{1-1/n_{macro}}} + \frac{e_{micro}}{\left[1+(D/d_{micro})^{n_{micro}}\right]^{1-1/n_{micro}}} \quad (2)$$

where: $d$ and $n$ are fitting parameters, $D$ is the pore diameter, macro and micro subscriptions stand for macro and micropore respectively.

### 2.3 Methodology for mechanical tests

16 saturated drained triaxial tests were performed in accordance with BS 1377:part 8 (BS, 1990). The samples were saturated using both percolation and counterpressure techniques until a B-value of 0.95 was achieved. They were then consolidated and sheared at a rate of 0.008 mm/min, as specified by BS 1377:part 8 (BS, 1990). Samples PN20 and PN28 were tested under four confining stresses: 50, 100, 200, and 400 kPa. Sample PN24 was tested under five confining stresses: 50, 75, 150, 300, and 600 kPa. Sample NP24 was tested under three confining stresses: 50, 100, and 200 kPa.

Additionally, 12 unsaturated tests were conducted following the constant water content (*CW*) method described by Rahardjo et al. (2004). The test is performed on undrained conditions with the pore air pressure kept constant while the pore water pressure increases while on shear. To ensure consistent drying paths, the samples were first moistened until they reached a water content corresponding to a suction of 50 kPa. The samples were then placed in the triaxial cell and subjected to a confining stress of 25 kPa. The water outlet was closed and increments of 10 kPa were applied to both pore air pressure and confining pressure until the desired pore air pressure was reached. The pore water pressure was then increased to achieve the target suction. The samples were consolidated under net stresses of 100 kPa and suctions of 50, 100, and 200 kPa, and then sheared at a rate of 0.017 mm/min with the water outlet closed to maintain constant water content, as per ASTM D4767 (ASTM, 2020).

## 3. Results and discussions

### 3.1 SWRC and MIP tests

Figure 3a,b shows the drying SWRC of the samples and Figure 4a shows the pore size distribution curve. The $R^2$ ranged from 0.96 to 0.99. The tests revealed that the samples exhibited bimodal characteristics under all compaction conditions. However, while water content and compaction energy significantly influenced the macropore region, the micropores remained essentially unchanged across all samples (Figure 4b and c). This behavior was previously observed by previous studies (Cordão Neto et al., 2018; Kühn et al., 2021; Lopes et al., 2022).

The MIP results in the pore size distribution of the soil. SWRC represents the relationship between suction and the amount of water in the soil and is directly related to pore size and frequency. Therefore, MIP and SWRC are directly related. The main difference between the SWRC and MIP tests is related to the measurement of volume changes, in which MIP uses dry samples and therefore does not account for volumetric changes during the test, as noted by Otálvaro et al. (2016). Further discussions regarding the differences between the techniques are not within the scope of this work.

Lower compaction energy correlates with a higher macropore void ratio, as demonstrated by Sample NP24 (Figure 4c). Samples compacted under the same energy (PN20, PN24, PN28) exhibited macropore void ratios (Figure 4c)

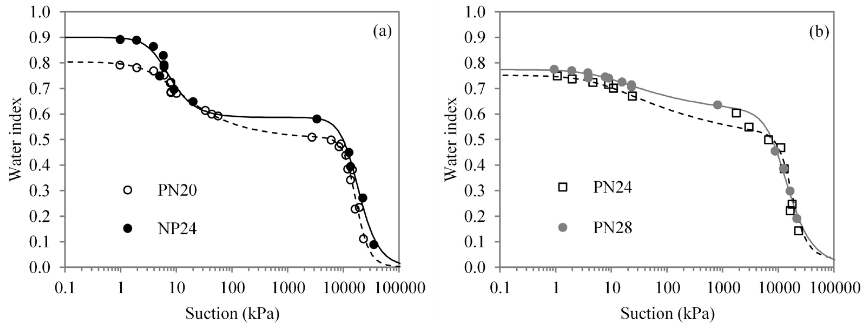


**Figure 3.** SWRC: (a) PN20 and NP24; (b) PN24 and PN28 (Modified from Otálvaro et al., 2016).

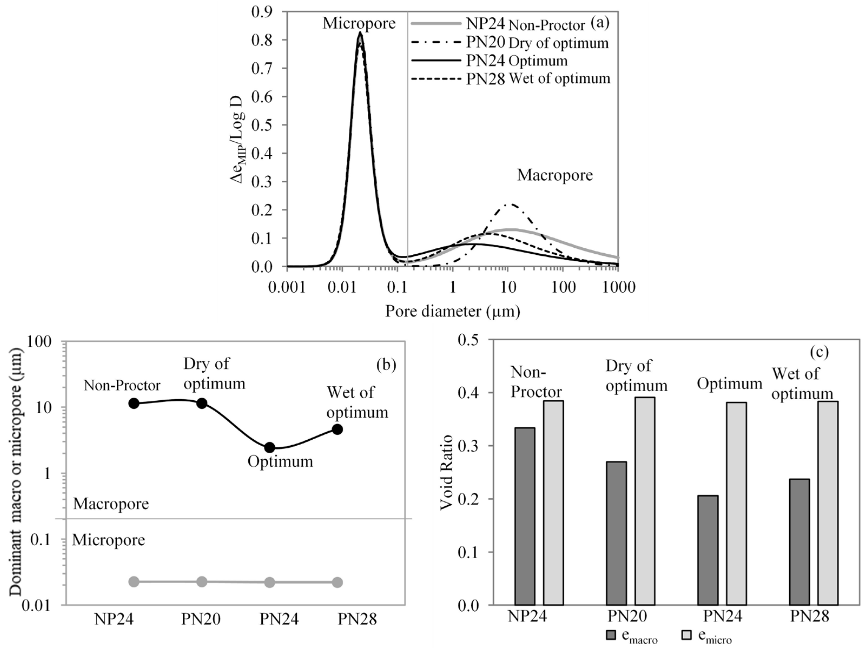


**Figure 4.** (a) Pore size distributions (Modified from Otálvaro et al., 2016); (b) Dominant macro and micro pore size; (c) Macro and micro pore void ratio.

and dominant macropore sizes (Figure 4b) that followed the compaction curve trend, with both values being smaller at optimum water content. Additionally, dry-side compaction resulted in higher void ratios and larger macropore sizes. This is similar to the results obtained by Santos & Esquivel (2018) and Lopes et al. (2022).

### 3.2 Saturated shear strength

Saturated triaxial tests were performed on 16 samples with varying water content and compaction conditions (Table 1). Figure 5 (a, b, c and d) shows the results for deviator stress x axial strain for all the samples on saturated condition. All samples exhibited similar behavior, with maximum deviator stress values ranging from 100 kPa to 1300 kPa as the consolidation stress increased. The shearing behavior was also similar, with all samples reaching the same stress levels and no peak deviator stress was observed. This result is expected, given the similar dry unit weights of the samples.

For the volumetric behavior during shearing (Figure 6a, b, c and d) the samples exhibited contractive behavior until reaching the critical state. The only exception was sample PN20_N50S0, which showed abnormal volumetric strain in the initial stages. While the system is automated, there is a potential for errors or initial reading discrepancies attributable to the measurement equipment. Nevertheless, it is understood that the triaxial system comprises several sub-components, suggesting that minor errors may occur without compromising the integrity of the entire test.

In Figure 7 is shown the consolidation phase results along with the Critical State Line (CSL). It was observed that while the samples compacted with the same water content resulted in a unique CSL (Figure 7a), the samples compacted with different water contents exhibited a different CSL (Figure 7b).

**Table 1.** Saturated triaxial test initial conditions.

| Sample | Stress (kPa) | Compaction Condition | $\gamma_d$ (kN/m$^3$) | $e$ | $W$ (%) |
|---|---|---|---|---|---|
| NP24_N50S0 | 50 | Non-Proctor | 13.9 | 0.34 | 24 |
| NP24_N100S0 | 100 | Non-Proctor | 13.9 | 0.34 | 24 |
| NP24_N200S0 | 200 | Non-Proctor | 13.9 | 0.34 | 24 |
| PN20_N50S0 | 50 | Dry Side | 14.0 | 0.26 | 20 |
| PN20_N100S0 | 100 | Dry Side | 14.0 | 0.26 | 20 |
| PN20_N200S0 | 200 | Dry Side | 14.0 | 0.26 | 20 |
| PN20_N400S0 | 400 | Dry Side | 14.0 | 0.26 | 20 |
| PN24_N50S0 | 50 | Optimum Water Content | 15.0 | 0.20 | 24 |
| PN24_N75S0 | 75 | Optimum Water Content | 15.0 | 0.20 | 24 |
| PN24_N150S0 | 150 | Optimum Water Content | 15.0 | 0.20 | 24 |
| PN24_N300S0 | 300 | Optimum Water Content | 15.0 | 0.20 | 24 |
| PN24_N600S0 | 600 | Optimum Water Content | 15.0 | 0.20 | 24 |
| PN28_N50S0 | 50 | Wet Side | 14.0 | 0.23 | 28 |
| PN28_N100S0 | 100 | Wet Side | 14.0 | 0.23 | 28 |
| PN28_N200S0 | 200 | Wet Side | 14.0 | 0.23 | 28 |
| PN28_N400S0 | 400 | Wet Side | 14.0 | 0.23 | 28 |

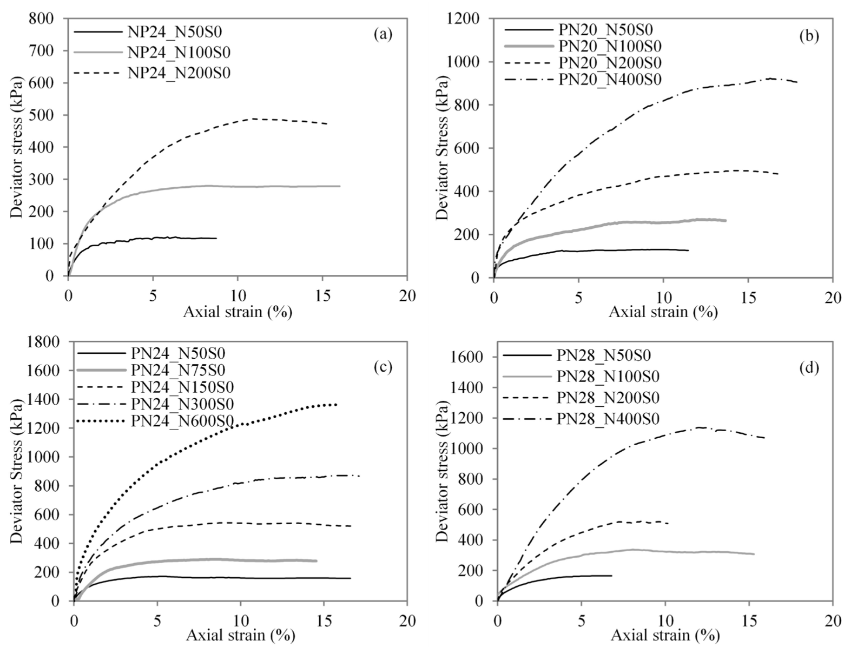


**Figure 5 .** Deviator stress x axial strain curves for saturated triaxial tests: samples (a) NP24; (b) PN20; (c) PN24; (d) PN28.

Figure 8a shows the CSL in the $e - lnp'$ space for all the samples, indicating that the critical state for all the saturated samples is practically unique, with sample PN20 displaying abnormal behavior. Notably, compaction on the dry side results in samples with higher void ratios on the critical state. Sample PN20 showed a higher void ratio after consolidation and exhibited less contraction during shearing. Both sample PN20 and NP24 had the largest dominant macropore diameters and the highest macropore void ratios, due to compaction on the dry side. This led to a uniform macropore distribution, which influenced the volumetric behavior of the saturated samples, especially on PN20.

For the CSL in the $p' - q$ space (Figure 8b), it was observed that the plot of mean effective stresses x deviator stress was not influenced by the compaction condition, resulting in a slope of the Critical State Line ($M$) equal to 1.35. This value corresponds to a friction angle of 33.6º, and have been previously observed in lateritic soil (Ng et al., 2020).

Wheeler & Sivakumar (2000) also observed a unique CSL and differences in the volumetric behavior for kaolinite samples under varying water content. Wang & Siu (2006)

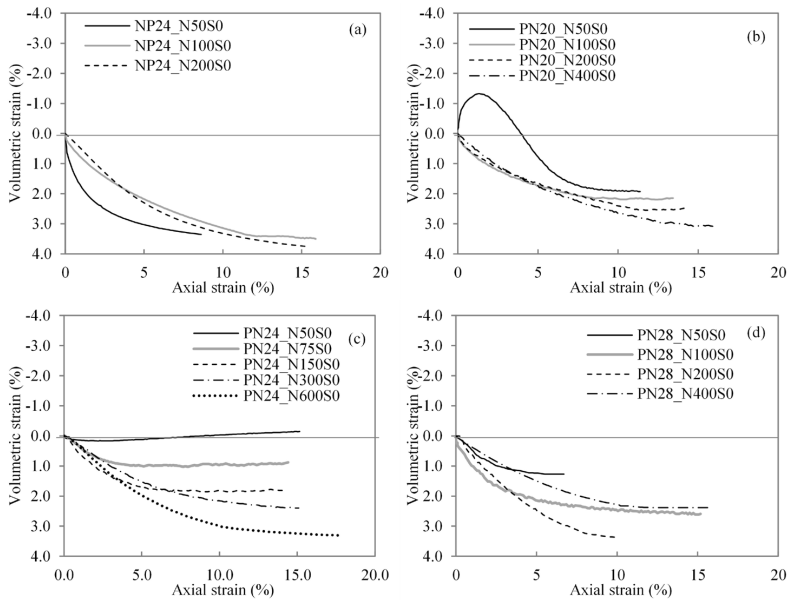


**Figure 6.** Volumetric strain x axial strain for saturated triaxial tests: samples (a) NP24; (b) PN20; (c) PN24; (d) PN28.

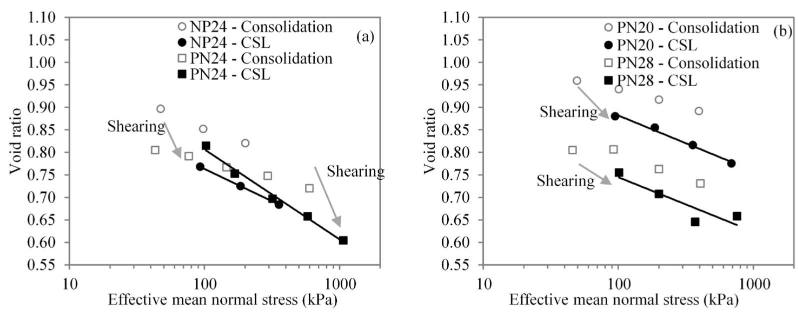


**Figure 7.** Consolidation results and Critical State Line plots for samples: (a) NP24 and PN24; (b) PN20 and PN28.

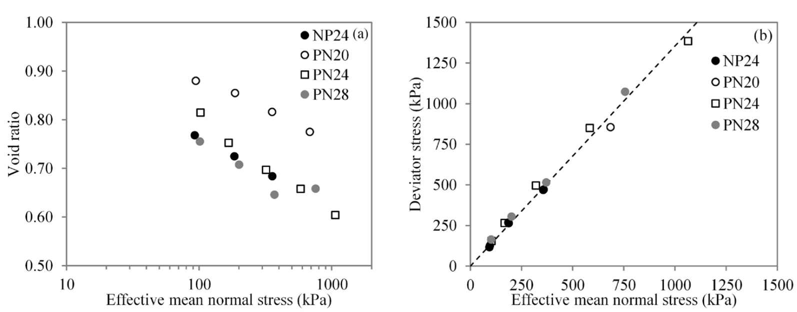


**Figure 8.** (a) Effective mean normal stress x void ratio on the critical state; (b) Effective mean normal x deviator stress on the critical state.

reported similar behavior in kaolin samples, where the structure was modified by *pH*.

Therefore, it can be presumed that, for both lateritic and non-lateritic soils, the friction angle at the critical state is not influenced by the soil structure. The Critical State Line (CSL) in the $p' - q$ space is essentially unique, but the volumetric behavior during shearing is affected by the initial pore size distribution. For this soil, the most significant effects on volumetric behavior are related to the dominant size and volume of the macropores.

### 3.3 Unsaturated shear strength

Unsaturated triaxial tests were performed on 12 samples with varying suction and compaction conditions, but with constant consolidation stress (Table 2). Figure 9a, b, c and d show the behavior of the deviator stress for samples NP24, PN24, PN20 and PN28 under unsaturated conditions. All the samples exhibited similar behavior with no peak deviator stress was observed. Increases in suction led to a general rise in maximum deviator stress, indicating an increase in shear strength.

Among the samples, PN24 and NP24, compacted with different compaction energies, showed the highest and lowest maximum deviator stresses values, respectively. Samples compacted with the same dry unit weight (PN20 and PN28) showed identical behavior, suggesting that the shear strength was mainly influenced by the dry unit weight. This highlights the significant role of both water content and compaction energy on the soil shear strength.

For the volumetric behavior during shearing (Figure 10a, b, c and d), samples NP24 and PN20 showed an overall contractive behavior, whereas samples PN24 and PN28 expanded during shear. This behavior is attributed to the higher macropores void ratio ( $e_{macro}$ ) of sample NP24, which allowed more voids to be compressed. Conversely, samples PN24 and PN28 had a smaller macropore void ratio, leading to expansion due to the lower availability of macro voids.

Additionally, the increase in suction resulted in a more pronounced dilatation behavior, as evidenced by the reduction in volumetric strain of the samples. Cementing agents also appear to play a fundamental role in shearing behavior. Particles aggregation tends to resist compression when loaded, leading to changes in soil structure and dilation when these macro pores are not available.

The results of apparent cohesion were fitted according to Vilar (2006) with an hyperbolic fit (Figure 11a), indicating that the increase in unsaturated shear strength with suction

**Table 2.** Unsaturated triaxial test initial conditions.

| Sample | Consolidation Stress (kPa) | Suction (kPa) | Compaction Condition | $\gamma_d$ (kN/m$^3$) | *e* |
|---|---|---|---|---|---|
| NP24_N100S50 | 100 | 50 | Non-Proctor | 13.9 | 0.34 |
| NP24_N100S100 | 100 | 100 | Non-Proctor | 13.9 | 0.34 |
| NP24_N100S200 | 100 | 200 | Non-Proctor | 13.9 | 0.34 |
| PN20_N50S50 | 100 | 50 | Dry Side | 14.0 | 0.26 |
| PN20_N100S100 | 100 | 100 | Dry Side | 14.0 | 0.26 |
| PN20_N200S200 | 100 | 200 | Dry Side | 14.0 | 0.26 |
| PN24_N100S0 | 100 | 50 | Optimum Water Content | 15.0 | 0.20 |
| PN24_N100S0 | 100 | 100 | Optimum Water Content | 15.0 | 0.20 |
| PN24_N100S0 | 100 | 200 | Optimum Water Content | 15.0 | 0.20 |
| PN28_N100S50 | 100 | 50 | Wet Side | 14.0 | 0.23 |
| PN28_N100S100 | 100 | 100 | Wet Side | 14.0 | 0.23 |
| PN28_N100S200 | 100 | 200 | Wet Side | 14.0 | 0.23 |

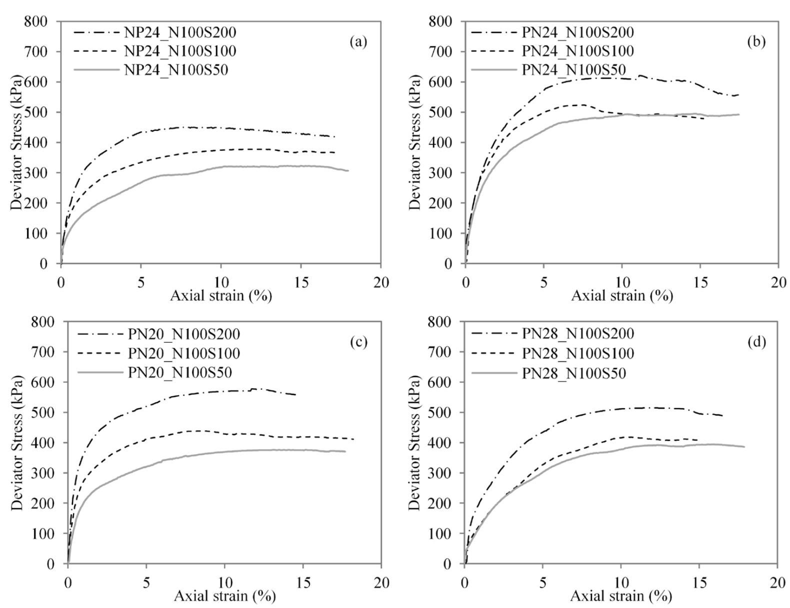


**Figure 9.** Deviator stress x axial strain plots for unsaturated samples: (a) NP24, (b) PN24, (a) PN20 and (d) PN28.

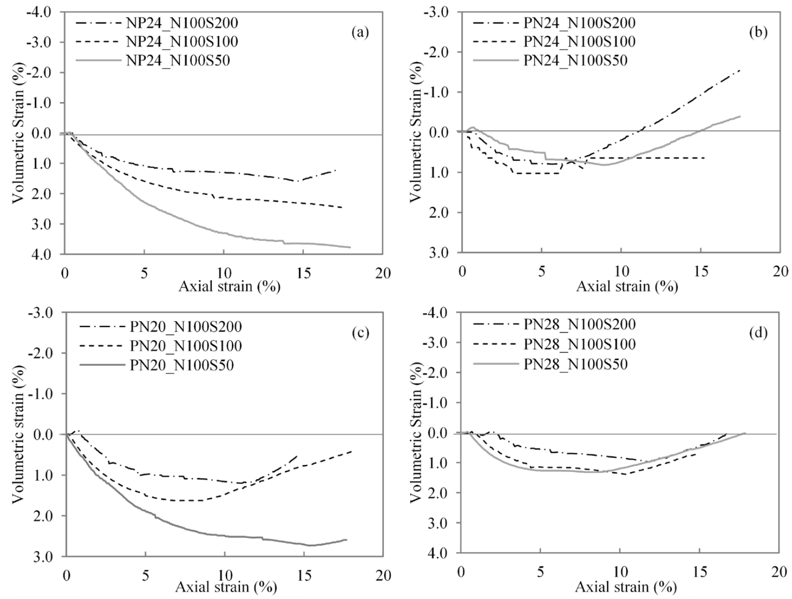


**Figure 10.** Volumetric strain x axial strain plots for unsaturated samples: (a) NP24, (b) PN24, (c) PN20 and (d) PN28.

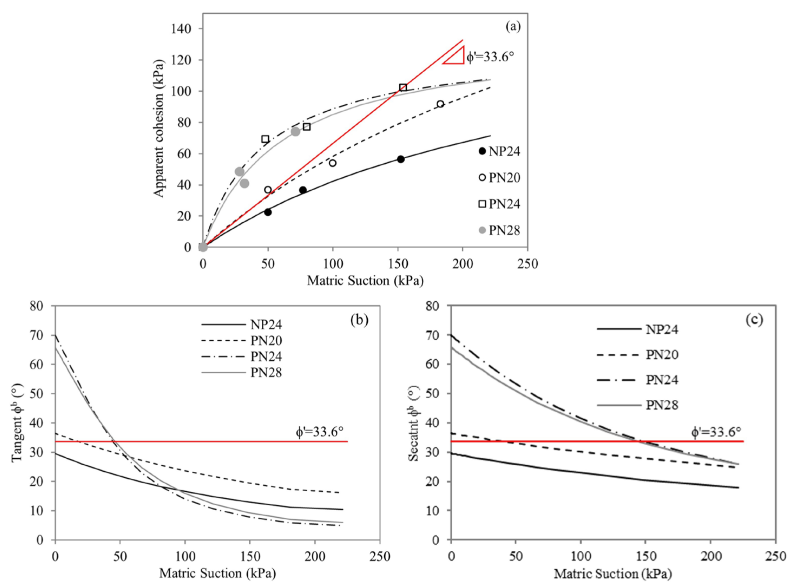


**Figure 11.**Variations in (a) apparent cohesion, (b) tangent angle, and (c) secant angle with suction.

is non-linear. This behavior was frequently observed in unsaturated soils, as noted by several authors (Gan et al., 1988, Vanapalli et al., 1996, Rassam & Williams, 1999). Additionally, the increase in cohesion with suction is very similar between samples PN24 and PN28, showing greater shear strength gains at lower initial suctions values.

Figure 11 also illustrates the variations in strength increase with suction ($\phi^b$) using both the tangent angle (Figure 11a) angle and the secant angle (Figure 11b), with the friction angle ($\phi'$=33.6°) as reference. The tangent is the line that touches the unsaturated shear strength curve in relation to matric suction at a single point, while the secant is the line that connects the origin to the point of interest on the unsaturated shear strength curve.

While samples NP24 and PN20 exhibited $\phi^b$ values lower than the friction angle ($\phi'$=33.6°), samples PN28 and PN24 showed higher $\phi^b$ values at initial suctions. This indicates a greater increase in strength due to suction compared to net stress. This behavior has been previously reported in tropical soils (Feuerharmel, 2007; Kühn, 2014; Pereira, 2006). An explanation for this behavior may be related to SWRC. As reported in previous articles, shear strength under unsaturated

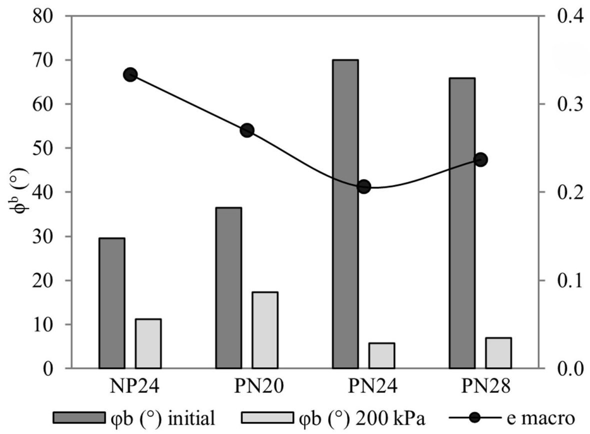


**Figure 12.** Relationship between $\phi^b$ and macropore void ratios.

conditions is directly related to SWRC (Fredlund et al., 1996; Vanapalli et al., 1996). The samples with similar SWRCs, such as PN24 with PN28 and NP24 with PN20, exhibited similar mechanical behaviors. Samples NP24 and PN20 demonstrated smaller increases in shear strength, likely due to their larger macropores sizes.

Figure 12 shows the relationship between the macropore void ratio and the $\phi^b$ angle at initial suctions and at a suction of 200 kPa. It was observed that the macropore void ratio correlates with suction, with smaller void ratios associated with higher unsaturated shear strength. While this behavior was pronounced at lower suctions, as suction increased, $\phi^b$ values tended to converge.

Therefore, it is concluded that the relationship of the SWRC with the mechanical behavior of an unsaturated sample is significant. All the samples under the compaction conditions studied have very similar micropores (Figure 3 and Figure 4). When the suction is increased, the SWRC gets closer in the micropore region, i.e., they have similar water content, resulting in an increase in shear strength between the samples.

## 4. Summary and conclusions

This paper evaluated the effects of the soil structure on the saturated and unsaturated shear strength of a lateritic soil compacted under different conditions. The compaction conditions influenced both pore size distribution and the Soil Water Retention Curve (SWRC). The Mercury Intrusion Porosimetry (MIP) revealed that all the samples exhibited a bimodal pore distribution. While macropores were significantly affected by compaction (water and energy), micropores remained practically unchanged. Samples compacted on the wet side of the compaction curve had lower macropore void ratios and smaller dominant pore diameters. Conversely, samples compacted on the dry side, or with non-proctor energy (less than Proctor), showed larger dominant pore diameter and greater macropore void ratios.

This structural modification impacted the saturated shear strength, particularly in terms of volumetric behavior. Samples compacted on the dry side exhibited larger dominant macropore diameters and a more uniform macropore distribution, which altered the Critical State line (CSL). This initial pore distribution led to higher void ratios at the critical state. However, samples compacted at optimum water content, on the wet side, or with non-proctor energy exhibited similar void ratios at the critical state.

It was also observed that the projection of the critical state line on the $p'$ x $q$ plane under saturated conditions resulted in an unique line with a slope of $M = 1.35$, regardless of the compaction condition. This behavior has been reported by other authors in both lateritic and non-lateritic soils.

Regarding shear strength behavior under unsaturated conditions, samples compacted on the dry side, wet side, and compacted with non-proctor energy showed contractive behavior during shearing. In contrast, samples compacted at optimum water content exhibited a decrease followed by a subsequent increase in volume. This is due to the smaller macropores void ratios, which led to an increase in volume during shear. Aggregates with cementing agents in tropical soils under unsaturated conditions do not compress during shear, leading to a decrease in the macropores void ratio or dilation when these pores are not available.

The increases in apparent cohesion with suction exhibited hyperbolic behavior, but the extent of strength gain varied on the pore distribution. This behavior is directly related to the SWRC. Samples with larger macropores void ratios showed less gain in shear strength gain at initial suction compared to samples with smaller macropores. This indicates that, even under unsaturated conditions, a reduction in macropores can improve shear strength in soils with a bimodal pore structure. In some cases, $\phi^b$ values at initial suctions were higher than $\phi'$. However, as suction increased, the water content and the micropore void ratio tended to become similar across samples, resulting in a more consistent increase in shear strength among the samples.

Given the inherent variability of soil behavior, especially soils with high mineralogical variability, some variability may be introduced into the experimental data. Despite this, the data is consistent with those observed in other studies.

This study demonstrated that compaction conditions significantly affect the pore structure and shear strength of tropical soil, particularly under unsaturated conditions. This has a relevant impact on engineering designs involving unsaturated compacted lateritic soils, such as earth dams, pavement subgrade, slope stability and earth structure designs in tropical climates. Future research should consider conducting unsaturated shear strength tests on samples compacted with higher compaction energies to reduce macropores. This approach will help assess the impact of micropores and cementing agents on the shear strength of tropical soils.

Moreover, the inclusion of large-scale tests could enhance practical utility and comparing these findings with other soil types (such as non-lateritic residual soils) might help generalize results. Additionally, developing specific models for these soils is recommended due to their unique characteristics.

## Acknowledgements

The authors would like to thank the Geotechnics program of Universidade de Brasília and Universidade Federal do Oeste da Bahia for the support provided to carry out this research as well as Universidad de Los Andes. The authors would also like to acknowledge the Brazilian research council, the National Council for Scientific and Technological Development (CNPQ) for providing the funds for providing the financial support for this research.

## Declaration of interest

The authors have no conflicts of interest to declare. All co-authors have observed and affirmed the contents of the paper and there is no financial interest to report.

## Authors' contributions

Ivan Fernando Otálvaro: conceptualization, data curation, visualization, investigation, methodology, validation, formal analysis. Vinícius de Oliveira Kühn: visualization, writing – original draft, writing – review & editing, validation, formal analysis. Bruno Leite Ramires Saldanha: writing – original draft, writing – review & editing, formal analysis. Bernardo Caicedo: project administration, resources. Manoel Porfirio Cordão Neto: conceptualization, visualization, methodology, formal analysis, writing – review & editing, supervision, project administration.

## Data availability

The datasets generated analyzed in the course of the current study are available from the corresponding author upon request.

## Declaration of use of generative artificial intelligence

This work was prepared without the assistance of any generative artificial intelligence (GenAI) tools or services. All aspects of the manuscript were developed solely by the authors, who take full responsibility for the content of this publication.

## List of symbols and abbreviations

| | |
|---|---|
| $a$ | Fitting parameter of SWRC |
| $d$ | Fitting parameter of SWRC |
| $e$ | Void ratio |
| $e_{macro}$ | Void ratio of macropores |
| $e_{micro}$ | Void ratio of micropores |
| $e_{mip}$ | Void ratio of MIP test |
| $e_w$ | Water index |
| $n$ | Fitting parameter of SWRC |
| $p'$ | Effective mean normal stress |
| $pH$ | Potential of hydrogen |
| $q$ | Deviator stress |
| s | Small pores of SWRC |
| $u_a$-$u_w$ | Matric suction |
| $w$ | Water content |
| $w_l$ | Liquid limit |
| CSL | Critical State Line |
| CW | Triaxial test with constant water content |
| $D$ | pore diameter |
| $G_s$ | Specific gravity |
| L | Large pores of SWRC |
| $M$ | Frictional constant |
| MIP | Mercury Intrusion Porosimetry |
| ML | Low plasticity silt |
| NP24 | Sample compacted at 20% water content and non Proctor energy |
| $PI$ | Plasticity index |
| PN20 | Sample compacted at Proctor energy with 20% water content |
| PN24 | Sample compacted at Proctor energy with 24% water content |
| PN28 | Sample compacted at Proctor energy with 28% water content |
| $S$ | Suction |
| SWRC | Soil Water Retention Curve |
| USCS | Unified Soil Classification System |
| XRD | X-ray diffraction |
| $\gamma_d$ | Dry unit weight |
| $\sigma_1$-$\sigma_3$ | Deviator stress |
| $\phi'$ | Friction angle |
| $\phi^b$ | Angle of strength increase relative to suction |

## References

Alonso, E.E., Pinyol, N.M., & Gens, A. (2013). Compacted soil behaviour: initial state, structure and constitutive modelling. *Geotechnique*, 63(6), 463-478. https://doi.org/10.1680/geot.11.P.134.

Alonso, E.E., Vaunat, J., & Gens, A. (1999). Modelling the mechanical behaviour of expansive clays. *Engineering Geology*, 54(1-2), 173-183. https://doi.org/10.1016/S0013-7952(99)00079-4.

ASTM D4767-11. (2020). *Standard Test Method for Consolidated Undrained Triaxial Compression Test for Cohesive Soils*. ASTM International, West Conshohocken, PA.

ASTM D698-12e2. (2012). *Standard Test Methods for Laboratory Compaction Characteristics of Soil Using*

*Standard Effort (12 400 ft-lbf/ft3 (600 kN-m/m3)*. ASTM International, West Conshohocken, PA.

BS 1377-8. (1990). *Methods of test for Soils for civil engineering purposes - Part 8: Shear strength tests (effective stress)*. British Standards Institution, London, UK.

Burland, J.B. (1990). On the compressibility and shear strength of natural clays. *Geotechnique*, 40(3), 329-378. https://doi.org/10.1680/geot.1990.40.3.329.

Camapum de Carvalho, J., & Gitirana, G. (2021). Unsaturated soils in the context of tropical soils. *Soils and Rocks*, 44(3), 1-25. https://doi.org/10.28927/SR.2021.068121.

Chandler, R.J., Crilly, M.S., & Smith, M.G.M. (1992). A low-cost method of assessing clay desiccation for low-rise buildings. *Proceedings of the Institution of Civil Engineers. Civil Engineering*, 92(2), 82-89. https://doi.org/10.1680/icien.1992.18771.

Cordão Neto, M.P., Hernández, O., Lorenzo Reinaldo, R., Borges, C., & Caicedo, B. (2018). Study of the relationship between hydro-mechanical soil behavior and microstructure of a structured soil. *Earth Sciences Research Journal*, 22(2), 91-101. https://doi.org/10.15446/esrj.v22n2.65640.

Delage, P., Audiguier, M., Cui, Y.-J., & Howat, M.D. (1996). Microstructure of a compacted silt. *Canadian Geotechnical Journal*, 33(1), 150-158. https://doi.org/10.1139/t96-030.

Delage, P., Marcial, D., Cui, Y.J., & Ruiz, X. (2006). Ageing effects in a compacted bentonite: a microstructure approach. *Geotechnique*, 56(5), 291-304. https://doi.org/10.1680/geot.2006.56.5.291.

Di Stefano, C., Ferro, V., & Mirabile, S. (2010). Comparison between grain-size analyses using laser diffraction and sedimentation methods. *Biosystems Engineering*, 106(2), 205-215. https://doi.org/10.1016/j.biosystemseng.2010.03.013.

Diamond, S. (1970). Pore size distributions in clays. *Clays and Clay Minerals*, 18(1), 7-23. https://doi.org/10.1346/CCMN.1970.0180103.

Dong, H., Leung, A.K., Liu, J., Karimzadeh, A.A., & Chen, R. (2025). Hydrochar effects on the microstructure and hydromechanical behaviour of unsaturated compacted soils. *Journal of Rock Mechanics and Geotechnical Engineering*, 17(9), 6045-6053. https://doi.org/10.1016/j.jrmge.2025.03.028.

Durner, W. (1994). Hydraulic conductivity estimation for soils with heterogeneous pore structure. *Water Resources Research*, 30(2), 211-223. https://doi.org/10.1029/93WR02676.

Feuerharmel, C. (2007). *Condutividade hidráulica de solos coluvionares não saturados da formação Serra Geral* [Doctoral thesis]. Universidade Federal do Rio Grande do Sul.

Fredlund, D.G., Xing, A., Fredlund, M.D., & Barbour, S.L. (1996). The relationship of the unsaturated soil shear strength to the soil-water characteristic curve. *Canadian Geotechnical Journal*, 33(3), 440-448. https://doi.org/10.1139/t96-065.

Fredlund, D.G., Rahardjo, H., & Fredlund, M.D. (2012). *Unsaturated soil mechanics in engineering*. John Wiley & Sons. https://doi.org/10.1002/9781118280492.

Futai, M.M., & Almeida, M.S.S. (2005). An experimental investigation of the mechanical behaviour of an unsaturated gneiss residual soil. *Geotechnique*, 55(3), 201-213. https://doi.org/10.1680/geot.2005.55.3.201.

Gan, J.K.M., Fredlund, D.G., & Rahardjo, H. (1988). Determination of the shear strength parameters of an unsaturated soil using the direct shear test. *Canadian Geotechnical Journal*, 25(3), 500-510. https://doi.org/10.1139/t88-055.

Gui, M.-W., & Yu, C.-M. (2008). Rate of strength increase of unsaturated lateritic soil. *Canadian Geotechnical Journal*, 45(9), 1335-1343. https://doi.org/10.1139/T08-065.

Kodikara, J., Islam, T., & Sounthararajah, A. (2018). Review of soil compaction: history and recent developments. *Transportation Geotechnics*, 17(15), 24-34. https://doi.org/10.1016/j.trgeo.2018.09.006.

Kühn, V.O. (2014). *Shear strength of an unsaturated tropical soil considering high suctions* [Master's dissertation]. Federal University of Goiás.

Kühn, V.O., Lopes, B.C.F.L., Borges, C.R., Massocco, N.S., & Cordão-Neto, M.P. (2021). Relationship between pore size distribution and compressibility of a lateritic soil. *Géotechnique Letters*, 11(4), 1-7. https://doi.org/10.1680/jgele.21.00063.

Kühn, V.O., Lopes, B.C.F.L., Caicedo, B., & Cordão-Neto, M.P. (2022). Mechanical behaviour of bimodal kaolin clay with aggregates. *Engineering Geology*, 297, 1-12. https://doi.org/10.1016/j.enggeo.2021.106490.

Lambe, T.W. (1958). The engineering behaviour of compacted clay. *Journal of the Soil Mechanics and Foundations Division*, 84(2), 1-35. https://doi.org/10.1061/JSFEAQ.0000115.

Lambe, T.W., & Whitman, R.V. (1969). Soil Mechanics, John Wiley and Sons. CRC Press, New York, New York, USA.

Leroueil, S., & Vaughan, P.R. (1990). The general and congruent effects of structure in natural soils and weak rocks. *Geotechnique*, 40(3), 467-488. https://doi.org/10.1680/geot.1990.40.3.467.

Li, P., Shao, S., & Vanapalli, S.K. (2020). Characterizing and modeling the pore-size distribution evolution of a compacted loess during consolidation and shearing. *Journal of Soils and Sediments*, 7(7), 2855-2867. https://doi.org/10.1007/s11368-020-02621-3.

Lopes, B.C.F.L., Cordão-Neto, M.P., & Tarantino, A. (2014). An approach to detect micro and macro-porosity from MIP data. In N. Khalili, A. Russell & A. Khoshghalb (Eds.), *Unsaturated soils: research & applications* (pp. 685–689) CRC Press. https://doi.org/10.1201/b17034-96.

Lopes, B.C.F.L., Kühn, V.O., Queiroz, Â.C.G., Caicedo, B., & Cordão-Neto, M.P. (2022). Structure evaluation of a tropical residual soil under wide range of compaction conditions. *Géotechnique Letters*, 12(2), 1-1. https://doi.org/10.1680/jgele.21.00101.

Marinho, F.A.M., & Oliveira, O.M. (2006). The filter paper method revisited. *Geotechnical Testing Journal*, 29(3), 250-258. https://doi.org/10.1520/GTJ14125.

Martins, E.S. (2000). *Petrografia, mineralogia e geomorfologia e rególitos lateríticos no Distrito Federal* [Doctoral thesis]. University of Brasília.

Miguel, M.G., & Bonder, B.H. (2012). Soil–water characteristic curves obtained for a colluvial and lateritic soil profile considering the macro and micro porosity. *Geotechnical and Geological Engineering*, 30(6), 1405-1420. https://doi.org/10.1007/s10706-012-9545-y.

Miguel, M.G., & Vilar, O.M. (2009). Study of the water retention properties of a tropical soil. *Canadian Geotechnical Journal*, 46(9), 1084-1092. https://doi.org/10.1139/T09-039.

Mitchell, J.K., & Soga, K. (2005). *Fundamentals of soil behavior* (3rd ed.). John Wiley and Sons.

Ng, C.W.W., Mu, Q.Y., & Zhou, C. (2017). Effects of soil structure on the shear behaviour of an unsaturated loess at different suctions and temperatures. *Canadian Geotechnical Journal*, 54(2), 270-279. https://doi.org/10.1139/cgj-2016-0272.

Ng, C.W.W., Akinniyi, D.B., & Zhou, C. (2020). Influence of structure on the compression and shear behaviour of a saturated lateritic clay. *Acta Geotechnica*, 15(12), 3433-3441. https://doi.org/10.1007/s11440-020-00981-1.

Nie, Y., Ni, W., Lü, X., Tuo, W., & Yuan, K. (2023). Macroscopic mechanical behavior and microstructural evolution of compacted loess in the Chinese Loess Plateau. *Soil & Tillage Research*, 232, 105767. https://doi.org/10.1016/j.still.2023.105767.

Otálvaro, I.F., Cordão-Neto, M.P., & Caicedo, B. (2015). Compressibility and microstructure of compacted laterites. *Transportation Geotechnics*, 5, 20-34. https://doi.org/10.1016/j.trgeo.2015.09.005.

Otálvaro, I.F., Neto, M.P.C., Delage, P., & Caicedo, B. (2016). Relationship between soil structure and water retention properties in a residual compacted soil. *Engineering Geology*, 205, 73-80. https://doi.org/10.1016/j.enggeo.2016.02.016.

Pereira, A. (2006). *Resistência ao cisalhamento de solos não saturados: análise experimental e teórica* [Master's dissertation]. Federal University of Rio Grande do Sul.

Prashant, A., & Penumadu, D. (2007). Effect of microfabric on mechanical behavior of kaolin clay using cubical true triaxial testing. *Journal of Geotechnical and Geoenvironmental Engineering*, 133(4), 433-444. https://doi.org/10.1061/(ASCE)1090-0241(2007)133:4(433).

Rahardjo, H., Heng, O.B., & Choon, L.E. (2004). Shear strength of a compacted residual soil from consolidated drained and constant water content triaxial tests. *Canadian Geotechnical Journal*, 41(3), 421-436. https://doi.org/10.1139/t03-093.

Rassam, D.W., & Williams, D.J. (1999). A relationship describing the shear strength of unsaturated soils. *Canadian Geotechnical Journal*, 36(2), 363-368. https://doi.org/10.1139/t98-102.

Santos, R.A., & Esquivel, E.R. (2018). Saturated anisotropic hydraulic conductivity of a compacted lateritic soil. *Journal of Rock Mechanics and Geotechnical Engineering*, 10(5), 986-991. https://doi.org/10.1016/j.jrmge.2018.04.005.

Tarantino, A., & De Col, E. (2008). Compaction behaviour of clay. *Geotechnique*, 58(3), 199-213. https://doi.org/10.1680/geot.2008.58.3.199.

Tarantino, A., & Tombolato, S. (2005). Coupling of hydraulic and mechanical behaviour in unsaturated compacted clay. *Geotechnique*, 55(4), 307-317. https://doi.org/10.1680/geot.2005.55.4.307.

van Genuchten, M.T. (1980). A closed-form equation for predicting the hydraulic conductivity of unsaturated soils. *Soil Science Society of America Journal*, 44(5), 892-898. https://doi.org/10.2136/sssaj1980.03615995004400050002x.

Vanapalli, S.K., Fredlund, D.G., Pufahl, D.E., & Clifton, A.W. (1996). Model for the prediction of shear strength with respect to soil suction. *Canadian Geotechnical Journal*, 33(3), 379-392. https://doi.org/10.1139/t96-060.

Vilar, O.M. (2006). A simplified procedure to estimate the shear strength envelope of unsaturated soils. *Canadian Geotechnical Journal*, 43(10), 1088-1095. https://doi.org/10.1139/t06-055.

Wang, Y.H., & Siu, W.K. (2006). Structure characteristics and mechanical properties of kaolinite soils. II. Effects of structure on mechanical properties. *Canadian Geotechnical Journal*, 43(6), 601-617. https://doi.org/10.1139/t06-027.

Wheeler, S.J., & Sivakumar, V. (2000). Influence of compaction procedure on the mechanical behaviour of an unsaturated compacted clay. Part 2: shearing and constitutive modelling. *Geotechnique*, 50(4), 369-376. https://doi.org/10.1680/geot.2000.50.4.369.

Xu, X.T., Chen, X.L., Cai, Y.Q., & Xu, X. (2025). Microstructure and macro-mechanical properties of residual soil subjected to repeated hygroscopic cycles. *Frontiers in Earth Science (Lausanne)*, 13, 1528098. https://doi.org/10.3389/feart.2025.1528098.

Yu, C.Y., Chow, J.K., & Wang, Y.H. (2016). Pore-size changes and responses of kaolinite with different structures subject to consolidation and shearing. *Engineering Geology*, 202, 122-131. https://doi.org/10.1016/j.enggeo.2016.01.007.